Available online at www.sciencedirect.com
ScienceDirect
Journal of Nuclear Materials 362 (2007) 287–292
journal of nuclear materials
www.elsevier.com/locate/jnucmat

Mechanical properties–microstructure correlation in neutron irradiated heat-affected zones of austenitic stainless steels

R. Stoenescu [a,b,*], R. Schaeublin [a], D. Gavillet [b], N. Baluc [a]

[a] *Ecole Polytechnique Fédérale de Lausanne (EPFL), Centre de Recherches en Physique des Plasmas, Association EURATOM-Confédération Suisse, 5232 Villigen PSI, Switzerland*
[b] *Paul Scherrer Institute, 5232 Villigen PSI, Switzerland*

Abstract

The effects of neutron irradiation on austenitic stainless steels, usually used for the manufacturing of internal elements of nuclear reactors (e.g. the core shrouds), are the alteration of the microstructure, and, as a consequence, of the mechanical properties. The present study is aimed at extending knowledge upon the impact of neutron-irradiation on the heat-affected zone of welded materials, which was influenced by the thermal cycles upon fusion welding. An austenitic stainless steel weld type AISI 304 from a decommissioned experimental pressurised water reactor has been used in the present study. The welded material has been irradiated during 11 reactor cycles to a maximum dpa dose of 0.35 and a temperature of around 573 K. The mechanical properties and microstructure are determined on specimens from heat-affected zone and base materials, with different dose levels. The mechanical properties were determined by performing tensile tests on small flat specimens at two deformation temperatures: room temperature and about 573 K. The characterisation of the microstructure was made by transmission electron microscopy. The correlation between mechanical properties and microstructure after neutron irradiation is made using the dispersed obstacle hardening model. It was found that the measured radiation hardening cannot be explained solely by the presence of the irradiation-induced defects observed in TEM. Smaller irradiation-induced features not resolvable in TEM may also contribute to radiation hardening.

PACS: 81.05.Bx

1. Introduction

Irradiation-induced microstructure influences the mechanical properties of neutron-irradiated materials and, in particular, of austenitic stainless steels [1–5]. Numerous studies show an increase in the yield strength and a decrease of the uniform elongation in tensile tests, as the irradiation dose increases. The ultimate tensile strength also increases, to a lower extent. The yield strength and uniform elongation seem to saturate at about 700 MPa and at about 10% respectively, from a dpa dose of about 1 [6,7].

* Corresponding author. Present address: Institutt for Energiteknikk/OECD Halden Reactor Project, P.O. Box 173, N-1751 Halden, Norway. Tel.: +47 69 21 2357; fax: +47 69 21 2201.
E-mail address: ralucas@hrp.no (R. Stoenescu).

0022-3115/$ - see front matter © 2007 Elsevier B.V. All rights reserved.
doi:10.1016/j.jnucmat.2007.01.251

The irradiation-induced change in yield strength is usually assumed to be due to the formation of faulted interstitial loops, since they are the dominant microstructural features present in materials irradiated in light water reactors. Hardening can be estimated from the number density and the mean size of the loops, using the dispersed barrier hardening model [8–10], first developed by Seeger. Hardening of austenitic stainless steels is accompanied by a loss of uniform elongation.

Although the specific damage microstructure depends on the particularities of the stainless steel type and on the irradiation conditions, typical irradiation-induced microstructural features in austenitic stainless steels are the so-called 'black dots' or unidentified nanometric defects, Frank dislocation loops, cavities [1,2,8,11–14] and, according to some authors, stacking fault tetrahedra [15–18], though in limited amount relative to the rest.

The goal of this study is to better understand the effects of neutron irradiation on the mechanical properties of heat-affected zones of welds made of austenitic stainless steel.

2. Experimental

The materials used in the present study originate from the thermal shield of a decommissioned experimental pressurised water reactor, the BR-3, in Mol, Belgium. The thermal shield is a welded austenitic stainless steel which has been irradiated during 11 reactor cycles between 1962 and 1987. During that period the reactor has experienced 5000 effective full power days at 40 MW (electric power of 11.5 MW), with a coolant temperature in the range of 533–573 K [19]. As the BR-3 reactor was an experimental PWR, its operating temperature and power were lower than those of the new generation of PWRs. Therefore, the exposure conditions of the thermal shield material are comparable to the current exposure conditions in boiling water reactors (BWRs). The material used for the thermal shield was a stainless steel of the type 304, with the following chemical composition: 0.08% C, 0.75% Si, 2% Mn, 0.045% P, 0.03% S, 18.0% Cr, 8.0% Ni, and Fe for the balance (in wt%).

Two plates with the same thermal history and different accumulated doses – decreasing from the inner to the outer side of the reactor – were selected for study. One plate (Block A), referred to as the unirradiated material, was taken from the top of the thermal shield and it has accumulated a dpa dose between 1.3×10^{-4} and 1.3×10^{-5}. The other plate (Block B) was taken from the high neutron flux region and its dpa dose is varying between 0.35 and 0.12 [19]. The grain size was determined using optical microscopy observations and a larger grain size was found close to the fusion line (151 μm), as compared to the values far away from the fusion line (106.8 μm), for both Block A and Block B materials.

Tensile tests and transmission electron microscopy (TEM) observations were performed in order to study the evolution of the mechanical properties and microstructure due to welding and neutron irradiation. Specimens were prepared from the base material (BM) and heat-affected zone (HAZ) for both Block A and Block B. A sketch of the weld metal and HAZ samples positions is shown in Fig. 1. Because of the small extension of the HAZ, tensile tests were made in the frame of small specimen technology, using flat specimens with the so-called Pirex geometry. The gage section dimensions are 5.5 mm length, 2.5 mm wide and about 0.35 mm thickness. The stress–strain relationship was determined at room temperature in air and at ~573 K in argon flow, using a constant strain rate of $5\times10^{-4}\,s^{-1}$, in both unirradiated and irradiated conditions. Values of the different tensile test parameters, yield strength (YS), ultimate tensile strength (UTS), uniform elongation (UE), were averaged from a minimum of ten measurements in the case of the unirradiated BMs and the error bars

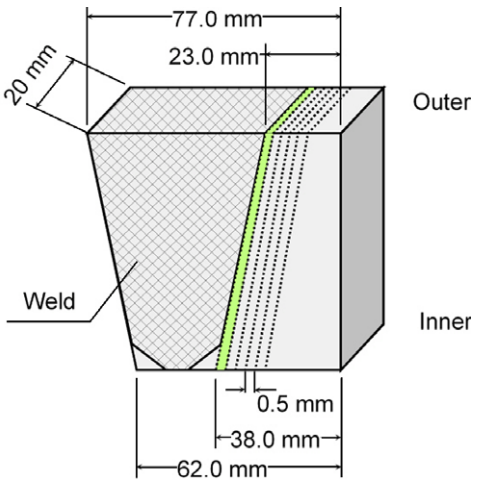

Fig. 1. Sketch of the weld metal and schematic of sample preparation from the HAZ. Specimens were cut along the FL, according to the dashed lines, under a 60° angle, corresponding to the weld edge preparation.

were determined from these values. For the HAZ, as well as for the irradiated materials, only one specimen was available per condition. The YS was measured at 0.2% plastic strain. The UTS corresponds to the maximum stress, where necking is expected to start. The UE was measured at the highest stress level, i.e. at the onset of necking.

TEM observations were performed using a JEOL 2010 microscope, operating at 200 kV, equipped with a detector for chemical analyses by X-ray energy dispersive spectrometry (EDS). The irradiation-induced defects were studied using dark-field and weak-beam dark-field imaging techniques. The defect size distribution of irradiation-induced defects was determined using series of micrographs imaged under different dark-field and weak beam conditions [20]. For thickness measurements the convergent beam electron diffraction (CBED) technique was applied. By using CBED, the foil thickness can be determined with an uncertainty of ±10% [21]. The error in the determination of loop number density is calculated as a sum of factors taking into account the statistical error, the foil thickness determination error and the error arising from the number of defects resolvable in TEM [22].

3. Results and discussion

Tensile tests were performed on small specimens from the HAZ and BM of the unirradiated and irradiated materials, at two deformation temperatures. Figs. 2 and 3 show the YS and UE variations with the irradiation dose and the distance from the FL. The YS presents higher values in the HAZ as compared to the BM, at both deformation temperatures. The YS is observed to decrease with increasing temperature. The UE values are lower in the HAZ as compared to the BM, at least for the specimens tested at room temperature. The UE is decreasing with increasing temperature. Hardening and loss of ductility are observed for both material states (BM and HAZ), at both testing temperatures.

The evolution of the microstructure in the HAZ in comparison with the BM was studied by TEM observations. Fig. 4 shows a bright field image in the case of the unirradiated material. The low dose material (Block A) exhibits a microstructure typical of austenitic stainless steels, with isolated dislocations and extended stacking faults. No irradiation-induced defects are visible in TEM. In Fig. 5 a weak-beam dark-field image in the case of irradiated material (Block B) is shown. When the irradiation

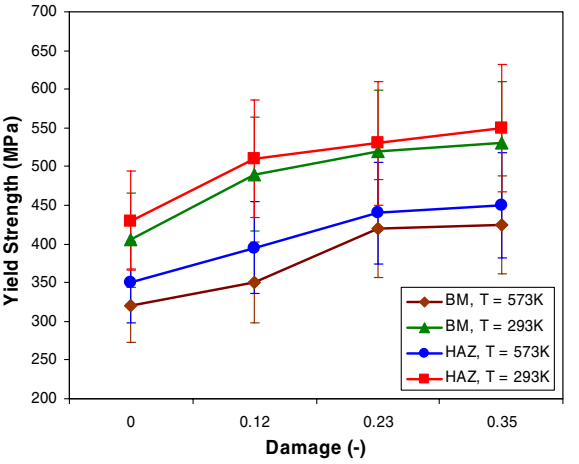

Fig. 2. Yield strength dependence on the irradiation dose for the BR-304 in-service material, base material and heat affected zone, at both testing temperatures.

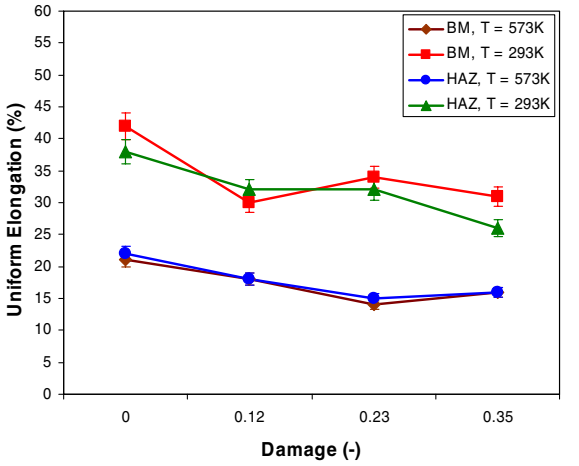

Fig. 3. Uniform elongation dependence on the irradiation dose for the BR-304 in-service material, base material and heat affected zone, at both testing temperatures.

dose is increased to a dpa of 0.35, irradiation-induced defects such as black dots and Frank dislocation loops are observed. The defect density and size distribution of irradiation-induced defects were determined using series of micrographs imaged under different weak-beam conditions and are reported in Table 1. A much higher defect density is observed in the HAZ than in the BM, but the dose dependence is not significant in this dose range. The higher defect density could be attributed to the successive heating and cooling phenomena that take place in the HAZ during the welding process, introducing residual stresses in the material.

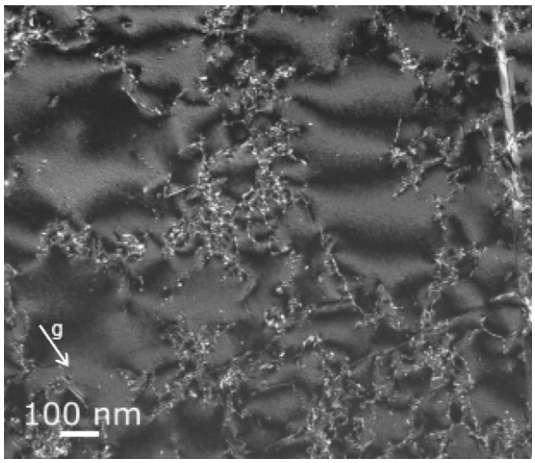

Fig. 4. Weak-beam image g(6 g), g {200}, close to a zone axis ⟨011⟩, of the low dose (Block A) BM (4 mm away from the fusion line) irradiated to a dpa dose of 1.3×10^{-4}.

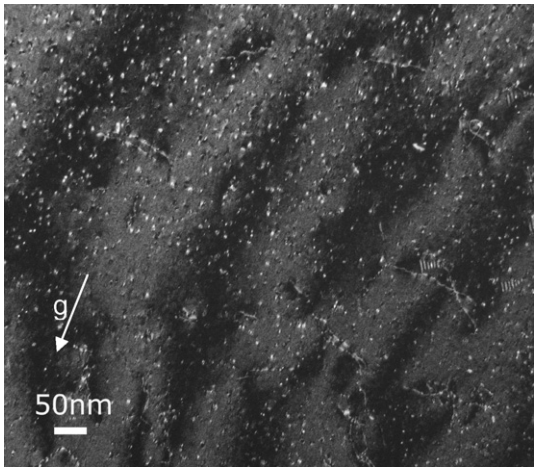

Fig. 5. Weak-beam image g(5 g), g {200}, close to a zone axis ⟨011⟩, of the high dose (Block B) BM (far away from the fusion line) irradiated to a dpa dose of 0.35.

The changes in mechanical properties of irradiated materials with respect to those of unirradiated ones are a direct consequence of the damage microstructure. Different models have been developed to understand the mechanical behaviour of irradiated materials from the microstructure evolution under irradiation. The dispersed barrier hardening model describes the increase in YS which is necessary in an irradiated material to move a dislocation through a field of irradiation-induced obstacles. The YS increase, or radiation hardening, defined as the difference between the YS of irradiated material and that of the unirradiated one is given by [10]:

$$\Delta\sigma_y = M \cdot \alpha \cdot \mu \cdot b \cdot \sqrt{N \cdot d} \quad (1)$$

where M is the Taylor factor that relates to the shear stresses in a slip plane of a single crystal to the tensile stresses necessary to activate slip in a polycrystalline material and it is equal to 3.06 for fcc materials [23], α is a value that characterises the obstacle strength, μ is the shear modulus, b is the modulus of the Burgers vector of the gliding dislocations, N is the number density and d is the mean size of obstacles, reported in Table 1. The Burgers vector is of the ⟨1 1 0⟩ type in fcc crystals [24] and its modulus was determined to be 0.257 nm [19]. The shear modulus has a value of 76.92 GPa [19].

To determine the values for the obstacle strength α, the radiation hardening $\Delta\sigma_y$ is plotted as a function of $(N \cdot d)^{1/2}$, by fitting the data with a straight line going through origin, as, by definition, radiation hardening is zero for unirradiated materials. The value of α can be determined from its slope, m, by using the following formula [25]:

$$\alpha = \frac{m}{M \cdot \mu \cdot b} \quad (2)$$

In Fig. 6 the radiation hardening is plotted against $(N \cdot d)^{1/2}$ in the case of irradiated BM, tested at 293 K. The resulting α value, calculated using Eq. (2) and Fig. 6, is 0.14.

The obstacle strength values, α, range usually between 0.1 and 1, depending on the barrier type [7,8,10,23,26]. For weak obstacles, such as small

Table 1
Defect density and mean size versus dose for the BM and HAZ of the high dose material (Block B)

Specimen and damage dose (dpa)	Black dots		Dislocation loops		Total defects	
	Density (m^{-3})	Mean size (nm)	Density (m^{-3})	Mean size (nm)	Density (m^{-3})	Mean size (nm)
BM 0.12	9.0×10^{21}	2.0	5.7×10^{21}	5.0	1.5×10^{22}	3.1
BM 0.35	1.7×10^{22}	2.0	6.7×10^{21}	4.0	2.4×10^{22}	2.5
HAZ 0.12	6.2×10^{23}	2.5	1.4×10^{23}	5.5	7.7×10^{23}	3.0
HAZ 0.35	5.2×10^{23}	2.5	2.9×10^{23}	4.5	8.1×10^{23}	3.2

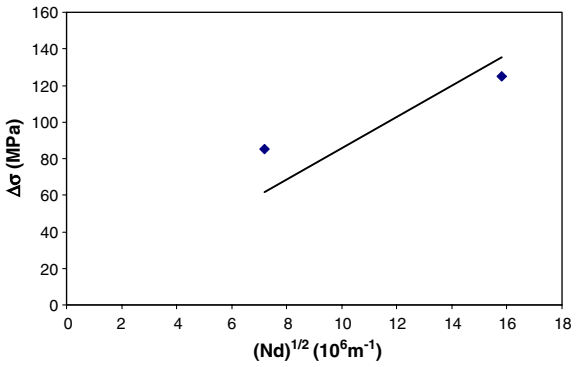

Fig. 6. Radiation hardening versus the square root of the product of the defect cluster density and their mean size for the base material irradiated at 293 K to dpa doses of 0.12 and 0.35.

loops and clusters, a value of 0.2 is usually used for α. For intermediate obstacles, such as Frank dislocation loops, $\alpha = 0.33$–0.4 [26]. So, the α values determined experimentally in the present study are small as compared to the ones found in the literature. With $\alpha = 0.14$, the irradiation-induced hardening in the case of BM tested at 293 K is calculated using Eq. (1) and a value of 66 MPa is found for a dpa dose of 0.35, which is lower than the experimental value of 125 MPa.

The difference could be attributed to the fact that the total change in YS has been calculated by using the total density and size of radiation-induced defects. It is not possible to separate the different contributions arising from different irradiation-induced defects, namely black dots and Frank dislocation loops.

In addition, one may assume that other irradiation-induced features, apart from black dots and Frank loops, also contribute to irradiation hardening. Then, the difference between the calculated values and the experimental ones could be due to a different radiation hardening behaviour occurring at low doses. It is assumed that small clusters, which cannot be detected by TEM, co-exist together with the observable irradiation-induced defects at small irradiation doses [26]. The non-observable defects have a different strength compared to the visible ones, so the linear fit going through origin exhibits a different slope at low doses.

4. Conclusions

The effects of neutron irradiation on the mechanical properties and microstructure of welded joints made of austenitic stainless steel have been investigated. The material was an AISI 304 type austenitic stainless steel from a decommissioned water reactor, which had accumulated a maximum dpa dose of 0.35 at about 573 K.

Studies of the mechanical properties of HAZs and BMs have been performed before and after irradiation and the following results were obtained. The HAZ shows higher strength and lower ductility as compared to the BM, at both testing temperatures (293 and 573 K). Neutron irradiation induces hardening and loss of ductility in all materials, at both testing temperatures.

Studies on microstructure of the irradiated materials show the presence of small black dots which cannot be identified in TEM and Frank dislocation loops. No stacking fault tetrahedra were observed. The irradiation-induced defect density was found to be higher in the HAZ as compared to the BM.

A correlation between the microstructure and the mechanical properties was established using the dispersed barrier hardening model. It was found that the irradiation-induced defects observed in TEM (black dots and Frank loops) are weak obstacles. Radiation hardening cannot be explained only by the presence of the irradiation-induced defects observed in TEM. Apparently, smaller defects, not resolvable in TEM, also contribute to radiation hardening.

Acknowledgement

This work was performed with the financial support of the European Commission, EURATOM FP5, contract number FIKS–CT–2000–00103, INTERWELD.

References

[1] T.S. Byun, K. Farrell, E.H. Lee, J.D. Hunn, L.K. Mansur, J. Nucl. Mater. 298 (2001) 269.
[2] N. Hashimoto, S.J. Zinkle, A.F. Rowcliffe, J.P. Robertson, S. Jitsukawa, J. Nucl. Mater. 283–287 (2000) 528.
[3] J.E. Pawel, A.F. Rowcliffe, D.J. Alexander, M.L. Grossbeck, K. Shiba, J. Nucl. Mater. 233–237 (1996) 202.
[4] J.L. Brimhall, J.I. Cole, S.M. Bruemmer, Scripta Metall. Mater. 30 (1994) 1473.
[5] T. Onchi, K. Dohi, N. Soneda, J.R. Cowan, R.J. Scowen, M.L. Castano, J. Nucl. Mater. 320 (2003) 194.
[6] K. Farrell, T.S. Byun, N. Hashimoto, J. Nucl. Mater. 335 (2004) 471.
[7] C. Bailat, The effect of light water reactor irradiation conditions of the microstructure and mechanical properties of stainless steel, Doctoral thesis, EPFL, 1999.

[8] S.J. Zinkle, Y. Matsukawa, J. Nucl. Mater. 329–333 (2004) 88.
[9] A.L. Bement Jr., Second International Conference on Strength of Metals and Alloys, American Society for Metals, Metals Park, OH, 1970, p. 693.
[10] G.E. Lucas, J. Nucl. Mater. 206 (1993) 287.
[11] M. Victoria, N. Baluc, C. Bailat, Y. Dai, M.I. Luppo, R. Schäublin, B.N. Singh, J. Nucl. Mater. 276 (2000) 114.
[12] J. Gan, G.S. Was, J. Nucl. Mater. 297 (2001) 161.
[13] N. Yoshida, J. Nucl. Mater. 174 (1990) 220.
[14] D.J. Edwards, E.P. Simonen, F.A. Garner, L.R. Greenwood, B.M. Oliver, S.M. Bruemmer, J. Nucl. Mater. 317 (2003) 32.
[15] D.J. Edwards, E.P. Simonen, S.M. Bruemmer, J. Nucl. Mater. 317 (2003) 13.
[16] Y. Dai, X. Jia, J.C. Chen, W.F. Sommer, M. Victoria, G.S. Bauer, J. Nucl. Mater. 296 (2001) 174.
[17] S.J. Zinkle, N. Hashimoto, D.T. Holezer, A.L. Quallas, T. Muroga, B.N. Singh, J. Nucl. Mater. 307–311 (2002) 192.
[18] M. Horiki, M. Kiritani, J. Nucl. Mater. 246 (1994) 212.
[19] R. Stoenescu, Effects of neutron irradiation on the microstructure and mechanical properties of the heat affected zones of stainless steel welds, Doctoral thesis, EPFL, 2005.
[20] D.J.H. Cockayne, I.L.F. Ray, M.J. Whelan, Philos. Mag. 20 (1969) 1265.
[21] J.H. Spence, J.M. Zuo, Electron Microdiffraction, Plenum, New York and London, 1992.
[22] M.L. Jenkins, M.A. Kirk, Characterisation of Radiation Damage by Transmission Electron Microscopy, Institute of Physics Publishing, Bristol and Philadelphia, 2001.
[23] X. Jia, The effects of simultaneous radiation damage and helium production on the microstructure and resulting mechanical properties of spallation source candidate materials, Doctoral thesis 2702, EPFL, 2003.
[24] D. Hull, D.J. Bacon, Introduction to Dislocations, Pergamon Press Ltd, 1984.
[25] N. Baluc, Y. Dai, M. Victoria, in: 20th Risø International Symposium on Materials Science, 1999, 245.
[26] R. Schäublin, D. Gelles, M. Victoria, J. Nucl. Mater. 307–311 (2002) 197.